ACS APPLIED POLYMER MATERIALS

pubs.acs.org/acsapm

Article

Boehmite Nanofiber–Polymethylsilsesquioxane Composite Macroporous Monoliths with High Diffuse Reflectance and Micromachinability

Gen Hayase*

Cite This: ACS Appl. Polym. Mater. 2025, 7, 10594–10600

Read Online

ACCESS | Metrics & More | Article Recommendations | Supporting Information

ABSTRACT: Boehmite nanofibers (BNF)-reinforced polymethylsilsesquioxane (PMSQ) composite macroporous monoliths were systematically optimized to achieve high diffuse reflectance, mechanical robustness, and machinability for optical applications. By varying the BNF content and methyltrimethoxysilane (MTMS) concentration, monolithic materials with controlled microstructures and tunable skeleton sizes were successfully fabricated. The optimized BNF–PMSQ monolith exhibited a diffuse reflectance of approximately 99.5% in the visible to near-infrared region of typical silicon photodiode detection (400–1100 nm), slightly exceeding the reflectance of the widely used diffuse polytetrafluoroethylene material (Spectralon). The improved mechanical properties facilitated precise machining by computer numerical control (CNC) milling and the fabrication of complex shapes using 3D printed molds owing to the chemical stability of the PMSQ matrix. The composite monolith exhibited surface hydrophobicity (static contact angle ∼ 155°) and thermal stability up to 350 °C without significant optical degradation, indicating potential suitability for outdoor applications. These results demonstrate that BNF–PMSQ macroporous monoliths are promising alternatives to traditional reflective materials, and combine environmental compatibility with high optical performance and versatile processing capabilities.

KEYWORDS: *polyorganosiloxanes, nanofibers, composites, macroporous monoliths, optical materials, diffuse reflectance, machinability, sol–gel*

1. INTRODUCTION

Diffuse reflectance materials play a crucial role in optical applications including spectroscopic calibration, optical detection enhancement, and the provision of uniform illumination inside integrating spheres. In optical metrology, the quality of the diffusive surface directly influences the accuracy and reliability of measurement systems. The recent surge in automated remote sensing, especially via drones and robotic inspection systems, has further increased the demand for reflective materials that are not only high performing but also durable and scalable.[1−3] In such applications, the stability and uniformity of the diffusive surface critically determine optical-calibration accuracy and consistent light distribution.

Currently, the most widely used diffuse reflectors include barium sulfate and porous polytetrafluoroethylene (PTFE)-based materials such as Spectralon.[4] Barium sulfate has been valued for its cost-effectiveness and high reflectance in the visible light range;[5,6] however, it is typically handled as a powder or additive and cannot be used as a bulk material as is. In contrast, PTFE-based materials have excellent reflectivity and remain stable over a wide range of wavelengths, including the near-infrared.[3,4,7−11] Despite these advantages, their high cost and complex manufacturing process hinder their widespread use, and environmental concerns about fluoropolymers[12] pose additional problems. These limitations have prompted the search for alternative materials that can provide comparable optical performance while also offering improved mechanical and environmental properties.[2,13] In addition, the growing demand for optical measurement systems to operate under harsh environmental conditions, including high temperature and humidity, requires the development of reflective materials with proven long-term durability in these challenging environments.

Silicone-based materials, particularly those with macroporous architectures, have emerged as promising candidates for next-generation diffuse reflectors due to their low absorption in the visible and near-infrared regions, excellent thermal and chemical stability, and mechanical robustness. Although few studies have investigated their diffuse reflectance in detail, several works have reported related optical functionalities such as radiative cooling

Received: May 16, 2025
Revised: July 5, 2025
Accepted: July 28, 2025
Published: August 1, 2025

https://doi.org/10.1021/acsapm.5c01749
ACS Appl. Polym. Mater. 2025, 7, 10594–10600

or spectral selectivity.[14−17] Our previous work[18,19] successfully demonstrated macroporous silicone macroporous monoliths with a diffuse reflectance exceeding 97.5% in the 400−1100 nm range, which is well within the detection range of standard silicon photodiode detectors. These materials were prepared using a sol−gel process incorporating tri- and difunctional silicon alkoxides, resulting in a porous structure capable of efficient backscattering. However, their inherent brittleness limited machinability and thus practical application in custom optical components or large-area reflective panels. To overcome these limitations, we turned to polysilsesquioxane-based porous materials, specifically boehmite nanofiber (BNF, AlOOH)[20,21]-reinforced polymethylsilsesquioxane (PMSQ, $CH_3SiO_{1.5}$) core−shell macroporous monoliths.[22,23] The incorporation of BNF into the PMSQ matrix significantly improves mechanical strength and crack resistance, outperforming conventional macroporous monolithic porous organosiloxane materials. This improved toughness allows for precision machining where computer numerical control (CNC) milling has been successfully applied to PMSQ macroporous monoliths to fabricate complex microstructures.[24] Such machinability is a critical advantage for optical applications that require customized reflective targets and integration with complex optical systems.

This study systematically optimizes the composition of BNF−PMSQ macroporous monoliths to maximize diffuse reflectance, mechanical integrity, and long-term stability while maintaining their high processability. Although the basic synthesis methodology remains unchanged, I refine the material properties through composition optimization and structural control. Furthermore, I validate the material's ability to undergo precise structural processing, demonstrating its feasibility for next-generation diffuse reflectors with superior optical performance and manufacturing versatility. By comparing the optical and physical properties of the optimized BNF−PMSQ monolith to Spectralon, I establish its potential as a low-cost, high-performance alternative. In addition, the absence of environmentally concerning fluoropolymers and the ability to fabricate complex geometries highlight the environmental and practical advantages of BNF−PMSQ monoliths over conventional materials. This research provides insight into the design of versatile diffuse reflectors, enabling broader applications in advanced optical technologies.

2. EXPERIMENTAL SECTION

Materials. A nanofiber sol, F-1000 (7.0 wt % in 2 M aqueous acetic acid), was obtained from Kawaken Fine Chemicals Co., Ltd., Japan. Its concentration was confirmed by drying at 80 °C for 24 h and measuring the residual mass. Methyltrimethoxysilane (MTMS) was supplied by Tokyo Chemical Industry Co., Ltd., Japan. Acetic acid, 2-propanol and limonene were all sourced from Kanto Chemical Co., Inc., Japan. All reagents were used as obtained without any further purification.

Sample Preparation. To prepare the monoliths, BNF dispersion sol F-1000 was first diluted x times (x = 5, 10, 20) in 100 mL of solution, resulting in final concentrations of 1.4 wt % (for x = 5), 0.70 wt % (for x = 10), and 0.35 wt % (for x = 20). Methyltrimethoxysilane (y mL; y = 50, 75, 100, 125, 150) was then added to the diluted sol, and the mixture was stirred for 15 min. After ultrasonic degassing, the mixture was poured into molds with an internal dimension of 115 mm × 115 mm, sealed, and allowed to gel at 75 °C for several hours. After gelation, the wet gels were heated for an additional 24 h. The resulting wet gels were then washed by immersion in 2-propanol for 24 h. After solvent exchange, the alcogels were evaporatively dried at 60 °C to yield samples designated BPx-y. A schematic overview of the preparation procedure is provided in Figure 1. The range of successfully obtained

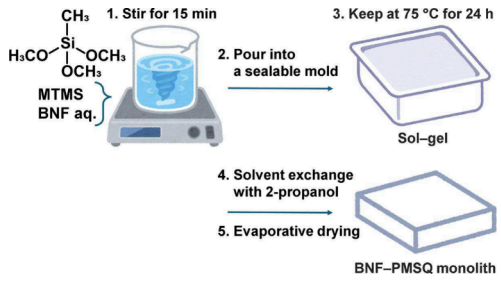

Figure 1. Schematic of the experimental procedure for fabricating BNF−PMSQ monoliths.

samples, which are defined as crack-free monoliths that retained their original shape after drying, and the conditions where sample formation failed are shown in Figure S1, Supporting Information. The IR and Raman spectra of BP10-100, a representative composition among the obtained samples, are shown in Figure S2, Supporting Information.

Shape Processing. BNF−PMSQ monoliths were formed by micromilling and 3D-printed molds. Micromilling was performed using a Kitmill CL200 (ORIGINALMIND Co., Ltd., Japan) equipped with a 1 mm diameter long neck ball end mill. BNF−PMSQ panels were fixed to the machine stage using 3 M double-sided tape during machining. 3D data representing the area around Mt. Fuji, downloaded as STL files from GSI Maps (Geospatial Information Authority of Japan; https://maps.gsi.go.jp/), were used for machining. The tool paths for three-dimensional machining were generated using Computer Aided Manufacturing (CAM) software Cut3D (Vectric Ltd., UK). For molding, a high-impact polystyrene (HIPS) mold was fabricated using a Flashforge Adventurer 4 (Zhejiang Flashforge 3D Technology Co., Ltd., China). The sol was poured into the mold, sealed with a film, vacuum degassed, and gelled in an oven. After gelation, the mold was removed by solvent exchange with 2-propanol and dissolution in limonene at 60 °C for 24 h. After dissolving the mold, the remaining material was subjected to another solvent exchange with 2-propanol, followed by evaporation drying at 60 °C to obtain the final product.

Characterization. Bulk density was determined by measuring the mass and dimensions of the panel-shaped monoliths. Prior to measurement, the surfaces were lightly polished with waterproof sandpaper to remove irregularities from mold release. The microstructure of the samples was observed using a field emission scanning electron microscope (FE-SEM) SU8000 (Hitachi High-Tech Corp., Japan). The Al:Si atomic ratio was evaluated by energy dispersive X-ray spectroscopy (EDX; Quantax FQ5060, Bruker, USA) attached to the FE-SEM. The skeletal diameter was analyzed using DiameterJ, a plugin for ImageJ, and the Super Pixel Diameter value was determined to one significant figure.[25,26] To observe cross sections of the microstructure, focused ion beam−scanning electron microscopy (FIB−SEM) was performed using an Ethos NX5000 (Hitachi High-Tech Corp., Japan). The samples were coated with carbon and milled using a Ga ion beam. Surface precision was measured with a Laser microscope VK-9700 (Keyence Corp., Japan). For molecular structure analysis, Fourier transform infrared spectroscopy (FTIR) was performed using IRSpirit-T (Shimadzu Corp., Japan) equipped with an ATR unit QATR-S. 100 scans of each sample were recorded at a resolution of 4 cm^{-1}. Additionally, micro-Raman spectroscopy was conducted using inVia Reflex (Renishaw plc, UK) with a laser wavelength of 532 nm and a grating of 1800 mm^{-1}. Optical measurements were performed on samples that were polished using waterproof sandpaper with an average particle size of 5 μm. Total reflectance measurement in the ultraviolet−visible-near-infrared (UV−vis−NIR) region was performed using a spectrophotometer V-770 (JASCO Corp., Japan) equipped with an integrating sphere unit ISN-923. Standard deviations from repeated reflectance measurements are provided in Figure S3 the Supporting Information. Angle-resolved measurements were performed using a spectrophotometer V-7200 (JASCO Corp., Japan) in combination with an automatic absolute reflectance measurement system VAR-7020. A diffuse reflectance standard (Spectralon SRS-99-010, Labsphere, Inc., USA) was used as a reflectance reference in all measurements.

https://doi.org/10.1021/acsapm.5c01749
ACS Appl. Polym. Mater. 2025, 7, 10594−10600

Midinfrared reflectance measurement was performed using a 10 cm gold-coated integrating sphere, Golden Eye III (Systems Engineering Inc., Japan), in combination with a Fourier transform infrared (FTIR) spectrometer IRTracer-100 (Shimadzu Corp., Japan). A diffuse gold coated mirror was used as the reference material. Uniaxial compression tests were performed using EZ Test EZ-SX (Shimadzu Corp., Japan) with a 500N gauge. The samples were cut into rectangular pieces with dimensions of 15 mm × 15 mm × 8 mm and used for the measurements. The crosshead speed was set at 1.0 mm min^{-1}. The Young's modulus was determined within the displacement range of 2.5% to 5.0%. Thermogravimetry−differential thermal analysis (TG−DTA) measurements were conducted using Thermo plus TG 8120 (Rigaku Corp., Japan). The measurements were performed under a flow of high-purity air at a rate of 100 mL min^{-1} with a heating rate of 10 °C min^{-1}. Open aluminum pans were used as the sample container, and α-alumina was employed as the reference material. Water droplet contact angles were measured using a custom-built device. Measurements were performed with 8.0 μL water droplets, deposited using a pen-type microsyringe pump SBP-100G-LLC (Takasago Electric, Inc., Japan). Contact angles were analyzed from images captured with a C-mount camera VCXU-02 M (Baumer Holding AG, Switzerland), equipped with a TECHSPEC 0.5X, 65 mm WD CompactTL telecentric lens (Edmund Optics Inc., USA) and a white LED backlight. Angles were determined using a custom program based on an ellipse-fitting method (source code provided in the Supporting Information). BELSORP-max (MicrotracBEL Corp., Japan) was used to measure the specific surface area by nitrogen gas adsorption and water vapor adsorption. Before measurement, each sample was degassed under vacuum at 110 °C for 12 h.

3. RESULTS AND DISCUSSION

3.1. Structure and Property Control of BNF−PMSQ Monoliths through Variation of Starting Composition. Skeleton size is an important factor in monolithic macroporous materials because light scattering depends on the size of the scattering medium.[27] In our previous studies of macroporous materials composed of polymethylsilsesquioxane (PMSQ) and silicone, we observed that when the skeleton diameter was significantly smaller than the wavelength of visible light, light scattering was suppressed, resulting in enhanced transmittance.[28−30] Conversely, when the skeleton size reached the micrometer scale, strong light scattering occurred, rendering the material white and opaque. In the case of BNF−PMSQ macroporous monoliths, increasing the amount of PMSQ added relative to BNF resulted in the growth of thicker skeletons. Therefore, I adjusted the BNF concentration and the MTMS mixing ratio in the initial composition to prepare samples with different structures. The physical properties and microstructures of the resulting samples are shown in Table 1 and Figure 2, respectively. Although the boehmite nanofibers are not directly visible in the SEM images due to their incorporation into the PMSQ skeleton, their presence could be indirectly observed through increased surface fibrillation after ball milling (Figure S4, Supporting Information).

Table 1. Starting Compositions and Physical Properties of the Crack-Free Monoliths Obtained

Sample	BNF aq. /wt %	MTMS/ mL	Bulk density /g cm^{-3}	Young's modulus /MPa	Si/Al atomic ratio
BP5-75	1.4	75	0.209	4.09	26.2
BP5-100	1.4	100	0.247	4.31	28.2
BP5-125	1.4	125	0.345	7.95	38.5
BP5-150	1.4	150	0.411	11.5	69.0
BP10-75	0.7	75	0.215	2.79	43.4
BP10-100	0.7	100	0.261	4.30	53.6

During sample preparation, excessively high concentrations of BNF inhibited skeleton formation and promoted aggregation, while excessively low concentrations resulted in uneven skeleton growth, making it difficult to produce homogeneous monoliths under either condition. All samples obtained exhibited fibrous or rod-like skeletons. These rod-like skeletons are expected to retain the previously confirmed core−shell structure, in which each boehmite nanofiber is coated with a PMSQ shell.[22,24] Notably, BP5-75 and BP10-100 had average skeleton sizes of 40 and 400 nm, respectively, a difference of more than 10-fold. I investigated how light scattering changes due to this difference in skeleton size. Integrating sphere measurements revealed significant differences in total reflectance among the samples due to variations in skeletal structure. Sample BP5-75, with the smallest skeletal diameter, exhibited a reflectance of over 98.5% in the visible region (400−800 nm); however, a significant decrease was observed in the near-infrared region (Figure 3). Conversely, BP10-100, which has the largest skeletal diameter, exhibited a relative total reflectance of 100.5% compared to Spectralon over the entire sensitivity range of a typical Si photodiode (400−1100 nm). This result indicates that the absolute reflectance of BP10-100 exceeds 99.5%. This enhancement is due to significant Mie scattering as the skeleton diameter equals or exceeds the wavelength of light in this region.[31,32] All samples exhibited absorption near 1200 nm, corresponding to the second overtone of C−H stretching vibrations. Beyond this wavelength, reflectance decreased due to various infrared absorptions, including those from the Si−OH stretching vibrations of the residual silanol groups. These results indicate that BNF−PMSQ monoliths, when limited to wavelengths below 1100 nm, exhibit total reflectance exceeding that of Spectralon, suggesting their potential as effective diffuse reflective materials.

3.2. Optical Reflectance Performance of BNF−PMSQ Macroporous Monoliths Compared with Spectralon. The bidirectional reflectance distribution function (BRDF) on a 2D plane of BP10-100, the sample with the highest total reflectance among the prepared BNF−PMSQ macroporous monoliths, was measured at a wavelength of 550 nm for incident angles of 5° and 45° and compared with that of Spectralon (Figure 4). At an incident angle of 5°, the BNF−PMSQ monolith exhibited slightly higher luminance than Spectralon over the entire detection angle range of −60° to 60°. At an incidence angle of 45°, the BNF−PMSQ monolith showed higher luminance than Spectralon in the −40° to 60° range. However, this trend was reversed in the −60° to −40° range, where Spectralon showed higher values. Overall, the difference in reflectivity between the two materials was small, although the BNF-PMSQ monolith showed higher retroreflection than Spectralon.

The differences in retroreflectivity between the BNF−PMSQ monolith and Spectralon appear to be largely due to their surface roughness. Higher roughness is known to increase retroreflectivity and thus strongly influence the perceived brightness of matte objects.[33] Roughness measurement using a laser microscope showed that even after precision polishing, the BNF−PMSQ monolith retained an arithmetic mean roughness (Ra) of ∼5 μm (Figure S5, Supporting Information), while Spectralon exhibited an Ra of ∼3 μm. Consistent with this correlation, preliminary BRDF measurements of the as-prepared, insufficiently polished BNF-PMSQ samples revealed an even stronger retroreflective component than that recorded after precision

https://doi.org/10.1021/acsapm.5c01749
ACS Appl. Polym. Mater. 2025, 7, 10594−10600

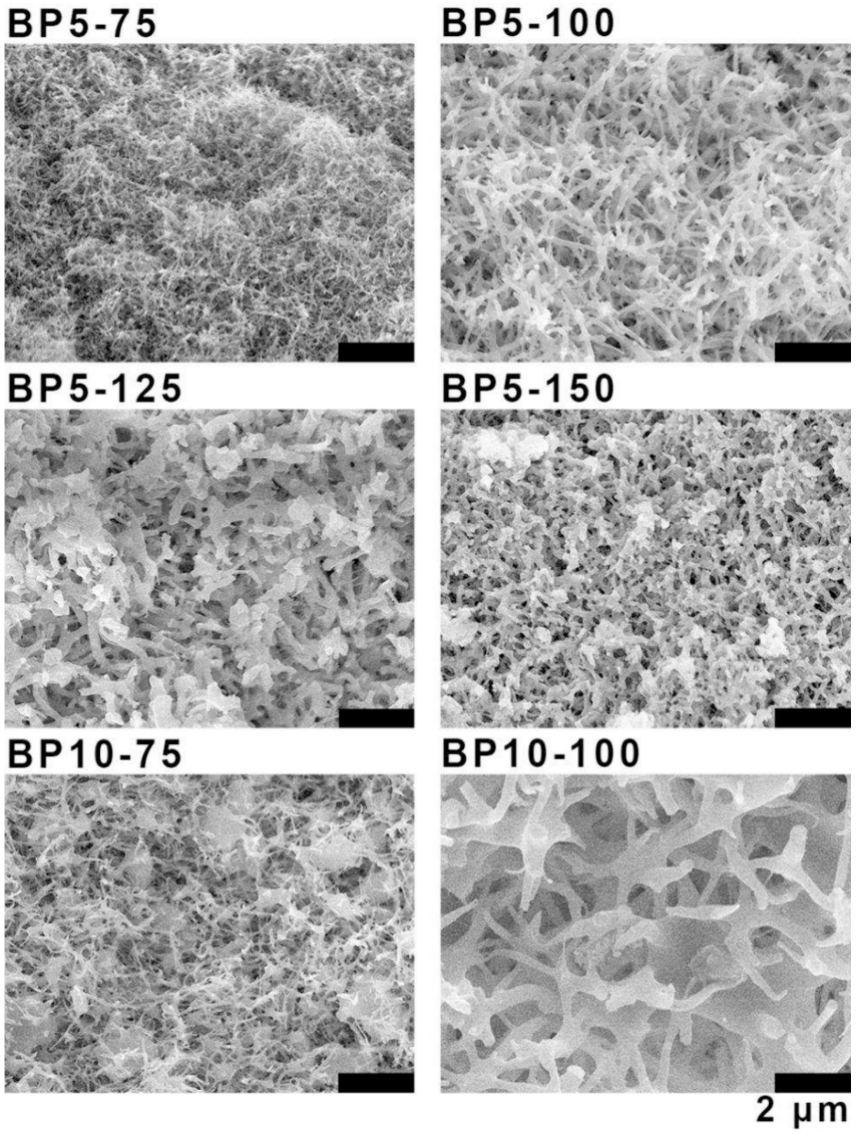

Figure 2. SEM images of BNF−PMSQ samples. Each scale bar indicates 2 μm.

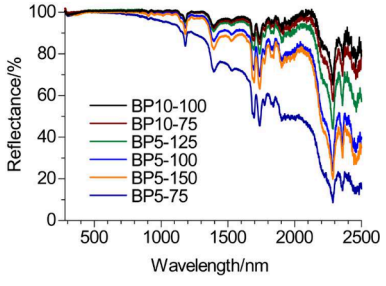

Figure 3. UV−vis−NIR spectra of BNF−PMSQ monoliths measured as relative total reflectance using Spectralon as a reference standard. Certain regions exceed 100%, indicating a higher reflectance than Spectralon.

polishing, suggesting that a coarser surface further enhances backscattering. However, differences in internal pore geometry may also contribute and warrant further investigation.

3.3. Surface Durability and Processability of BNF−PMSQ Monoliths. Spectralon, produced by compressing polytetrafluoroethylene (PTFE) powder, exhibits significant hydrophobicity, which facilitates wet polishing of surfaces. Similarly, BNF−PMSQ monoliths exhibit a considerable hydrophobicity, enabling effective wet polishing. Typically, highly porous materials are considered fragile and difficult to polish. However, the composite nature of BNF−PMSQ monoliths overcomes this challenge by providing sufficient mechanical strength to withstand the mechanical forces applied during polishing. Its adequate elasticity allows for secure mechanical clamping and pressure to be applied to the surface during polishing without causing damage. In a uniaxial compression test up to 60% of the original sample thickness (Figure 5 and Movie S1, Supporting Information), about 5% residual strain was observed immediately after unloading, but the sample gradually recovered over the course of several hours. This slow recovery is likely due to the heterogeneous porous structure, where thinner regions of the skeleton relax more slowly. The density of hydroxyl groups on the BNF−PMSQ monoliths, calculated from adsorption measurements, was 14% of the total specific surface area, based on BET specific surface areas of 156 $m^2 g^{-1}$ for nitrogen and 22.0 $m^2 g^{-1}$ for water. These values are indicative of hydrophobic properties, although not as pronounced as those observed in fluoropolymers. However, the micro- and nanoscale surface roughness is likely to contribute

https://doi.org/10.1021/acsapm.5c01749
ACS Appl. Polym. Mater. 2025, 7, 10594−10600

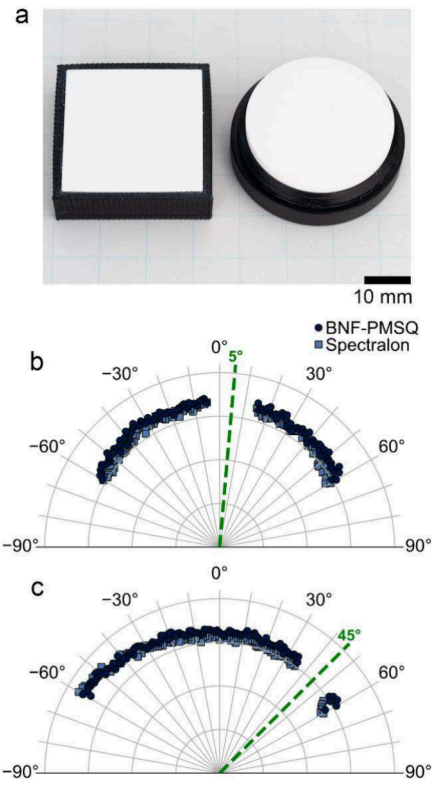

Figure 4. (a) Photograph of BNF−PMSQ monolith BP10-100 and Spectralon samples. Luminance distribution characteristics of BP10-100 and Spectralon for diffuse reflection: (b) at an incident angle of 5° and (c) at an incident angle of 45°.

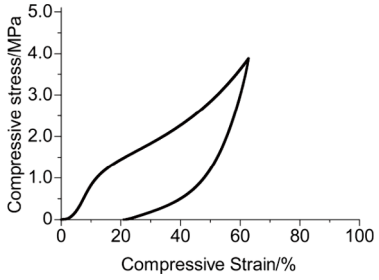

Figure 5. Stress−strain curve of BNF−PMSQ monolith BP10-100 under compression test. During the final stage of unloading, the shape recovery of the monolith did not keep pace with the crosshead speed of the testing machine. Approximately 5% residual strain was observed at the end of the test; however, the monolith gradually returned to its original shape within several hours.

significantly to the water repellency of the material.[14,15,34−39] The static water contact angle measured on the sample surfaces used for optical evaluation was 155°, corresponding to a superhydrophobic state. (Figure 6) However, it is important to note that this contact angle showed some variation depending on the polishing conditions. This hydrophobicity can reduce surface contamination and simplify maintenance for long-term outdoor use.

Thermogravimetric−differential thermal analysis (TG−DTA) showed that BNF−PMSQ monoliths exhibited no significant weight loss or thermal degradation up to approximately 400 °C, indicating structural stability at elevated temperatures (Figure 7). The optical performance of BNF−PMSQ monoliths remained largely unchanged after heating to

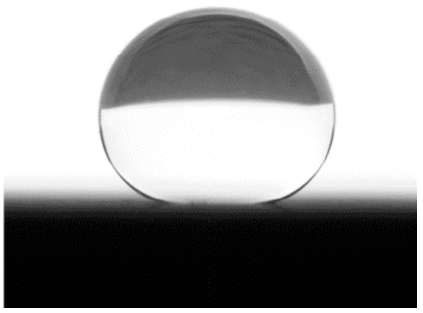

Figure 6. Water droplet (8.0 μL) on the BNF-PMSQ monolith; the static water contact angle was 155°.

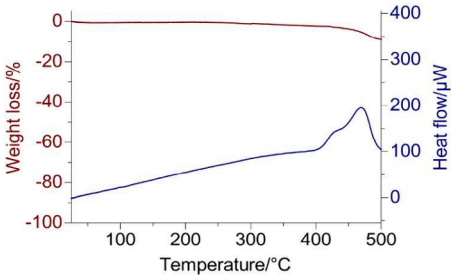

Figure 7. Thermogravimetric−differential thermal analysis (TG−DTA) curve of a BNF−PMSQ monolith BP10-100.

approximately 350 °C, demonstrating thermal stability comparable to that of Spectralon. These results suggest that BNF−PMSQ monoliths possess durability suitable for potential applications as diffuse reflective materials in optical measurement systems operating under severe conditions, such as exposure to high power light sources and high-temperature outdoor environments. In the future, radiation and other tests will be conducted with an eye toward space applications.

Spectralon is known for its exceptional diffuse reflection properties and is widely used in optical standards. While it can be machined into specific geometries, the fabrication of intricate or highly detailed structures remains limited due to the inherent rigidity and mechanical properties of the material. In contrast, BNF−PMSQ monoliths offer enhanced versatility for producing fine and complex geometries. Their compatibility with both CNC micromilling and solvent-removable 3D-printed molds enables the direct formation of detailed surface features and customized optical components (Figure 8). By taking advantage of the resistance of polyorganosiloxane to organic solvents, these monoliths can be fabricated using 3D-printed templates. In addition, their robust mechanical strength allows for precise CNC machining, achieving accuracies in the tens of micrometers. This adaptability facilitates customized material designs at the laboratory scale, such as the fabrication of integrating spheres and other optical devices. Furthermore, BNF−PMSQ monoliths hold promise for applications in solar reflective materials with a radiative cooling property, given their reflectivity over a range of wavelengths and mid-infrared emissivity at wavelengths of 8 to 13 μm (Figure 9).[14,15,34−39] Taken together, these properties highlight the potential of BNF−PMSQ monoliths as future diffuse reflective materials.

4. CONCLUSIONS

To overcome the limitations of existing diffuse reflective materials, the composition and structure of boehmite nanofiber (BNF)-reinforced polymethylsilsesquioxane (PMSQ) macro-

https://doi.org/10.1021/acsapm.5c01749
ACS Appl. Polym. Mater. 2025, 7, 10594−10600

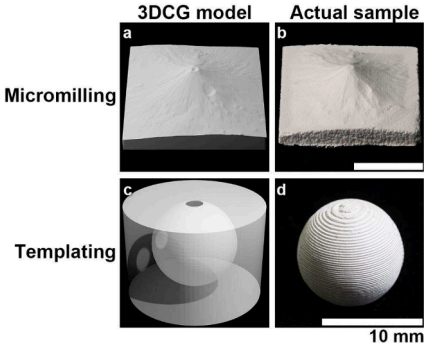

Figure 8. Microfabrication of BNF−PMSQ monoliths: (a) 3D-computer graphics (3DCG) model of the topographical surface; (b) sample fabricated via CNC micromilling; (c) 3DCG representation of the 3D-printed mold (a photograph of the actual mold is provided Figure S6, Supporting Information); (d) sample obtained by removing the mold with limonene. Even the filament layer lines of the 3D-printed mold are reproduced. Each scale bar indicates 10 mm.

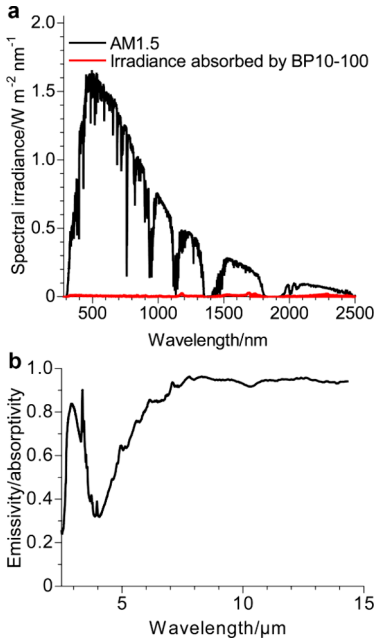

Figure 9. (a) Solar absorption irradiance calculated from total light reflectance of BNF−PMSQ monolith BP10-100 and air mass (AM1.5). (b) Midinfrared spectrum of BP10-100.

porous monoliths were systematically optimized. By adjusting the ratio of BNF to MTMS, precise control over microstructural properties such as skeleton size and porosity was achieved, allowing tuning of optical reflectance. The optimized BNF−PMSQ monolith exhibited a diffuse reflectance of approximately 99.5% over the spectral range relevant to silicon photodiodes (400−1100 nm), slightly exceeding the performance of the commercially available Spectralon material. The mechanical properties of the composite material facilitated precise machining, allowing wet polishing of the surface and fabrication of complex geometric structures. Thermogravimetric−differential thermal analysis demonstrated the thermal stability of the material up to approximately 400 °C with no noticeable degradation in optical properties. Given the intrinsic stability of silsesquioxane and ceramic-based materials, degradation under ambient conditions is expected to be minimal over the long-term.

These results demonstrate that BNF−PMSQ monoliths have the potential to serve as alternative diffuse reflectors to conventional materials, with potential applications including optical calibration systems and solar reflective coatings. Future research will specifically focus on extended environmental durability testing and scalability studies to further evaluate practical applicability.

■ ASSOCIATED CONTENT

Supporting Information

The Supporting Information is available free of charge at https://pubs.acs.org/doi/10.1021/acsapm.5c01749.

Diagram of the tested composition range; IR and Raman spectra; reflectance standard deviation data; FIB−SEM and ball-milled SEM images; surface roughness measurements; photograph of the 3D-printed HIPS mold; and Python code used for water contact angle calculation (PDF)

Mechanical deformation of BP10-100 during compression test (MP4)

■ AUTHOR INFORMATION

Corresponding Author

Gen Hayase − *Research Center for Electronic and Optical Materials, National Institute for Materials Science, Tsukuba, Ibaraki 305-0044, Japan;* orcid.org/0000-0003-1970-6129; Email: gen@aerogel.jp

Complete contact information is available at: https://pubs.acs.org/10.1021/acsapm.5c01749

Notes

The author declares no competing financial interest.

■ ACKNOWLEDGMENTS

The author thanks Mr. Cong Zhang and Dr. Masanobu Iwanaga (National Institute for Materials Science) for helping reflectance measurements. This work was supported by "Advanced Research Infrastructure for Materials and Nanotechnology in Japan (ARIM)" of the Ministry of Education, Culture, Sports, Science and Technology (MEXT). Proposal Number JPMXP1223NM5285, JPMXP1224NM5101, and JPMXP1225NM5072.

■ REFERENCES

(1) Suomalainen, J.; Oliveira, R. A.; Hakala, T.; Koivumaki, N.; Markelin, L.; Nasi, R.; Honkavaara, E. Direct reflectance transformation methodology for drone-based hyperspectral imaging. *Remote Sens. Environ.* **2021**, *266*, 112691.

(2) Sanches, I. D.; Tuohy, M. P.; Hedley, M. J.; Bretherton, M. R. Large, durable and low-cost reflectance standard for field remote sensing applications. *Int. J. Remote Sens.* **2009**, *30* (9), 2309−2319.

(3) Bruegge, C. J. Use of Spectralon as a diffuse reflectance standard for in-flight calibration of earth-orbiting sensors. *Opt. Eng.* **1993**, *32* (4), 805.

(4) Diffuse Reflectance Materials, Coatings, Targets, Standards. Labsphere. See the following: https://www.labsphere.com/product-category/materials-coatings-targets-standards/ (accessed Apr 1, 2025).

(5) Schutt, J. B.; Arens, J. F.; Shai, C. M.; Stromberg, E. Highly reflecting stable white paint for the detection of ultraviolet and visible radiations. *Appl. Opt.* **1974**, *13* (10), 2218−2221.

(6) Poh, A. H.; Jamaludin, M. F.; Fadzallah, I. A.; et al. Diffuse reflectance spectroscopic analysis of barium sulfate as a reflection

standard within 173−2500 nm: From pure to sintered form. *J. Near Infrared Spectrosc.* **2019**, *27* (6), 393−401.
(7) Bhandari, A.; Hamre, B.; Frette, Ø; Zhao, L.; Stamnes, J. J.; Kildemo, M. Bidirectional reflectance distribution function of Spectralon white reflectance standard illuminated by incoherent unpolarized and plane-polarized light. *Appl. Opt.* **2011**, *50* (16), 2431−2442.
(8) Tsai, B. K.; Allen, D. W.; Hanssen, L. M.; Wilthan, B.; Zeng, J. A comparison of optical properties between solid PTFE (Teflon) and (low density) sintered PTFE. In *Reflection, Scattering, and Diffraction from Surfaces*; Gu, Z-H, Hanssen, L. M., Eds.; SPIE, 2008; Vol. *7065*, pp 239−247. DOI: 10.1117/12.798138.
(9) Cone, M. T.; Musser, J. A.; Figueroa, E.; Mason, J. D.; Fry, E. S. Diffuse reflecting material for integrating cavity spectroscopy, including ring-down spectroscopy. *Appl. Opt.* **2015**, *54* (2), 334−346.
(10) Janecek, M.; Moses, W. W. Optical reflectance measurements for commonly used reflectors. *IEEE Trans. Nucl. Sci.* **2008**, *55* (4), 2432−2437.
(11) Weidner, V. R.; Hsia, J. J. Reflection properties of pressed polytetrafluoroethylene powder. *J. Opt. Soc. Am.* **1981**, *71* (7), 856−861.
(12) Wang, Z.; Cousins, I. T.; Scheringer, M.; Hungerbühler, K. Fluorinated alternatives to long-chain perfluoroalkyl carboxylic acids (PFCAs), perfluoroalkane sulfonic acids (PFSAs) and their potential precursors. *Environ. Int.* **2013**, *60*, 242−248.
(13) Yu, S.; Chen, J.; Gomard, G.; Hölscher, H.; Lemmer, U. Recent progress in light-scattering porous polymers and their applications. *Adv. Opt. Mater.* **2023**, *11* (13), 2203134.
(14) Zhao, H.; Sun, Q.; Zhou, J.; Deng, X.; Cui, J. Switchable Cavitation in Silicone Coatings for Energy-Saving Cooling and Heating. *Adv. Mater.* **2020**, *32* (29), No. e2000870.
(15) Zhou, L.; Rada, J.; Zhang, H.; et al. Sustainable and inexpensive polydimethylsiloxane sponges for daytime radiative cooling. *Adv. Sci.* **2021**, *8* (23), No. e2102502.
(16) Aoyama, T.; Sonoda, T.; Nakanishi, Y.; Tanabe, J.; Takebayashi, H. Study on aging of solar reflectance of the self-cleaning high reflectance coating. *Energy Build.* **2017**, *157*, 92−100.
(17) Zuo, T.; Zhang, J.; Zhong, S.; Xu, T.; Xu, L.; Xu, S.; Pan, B.; Cai, Y.; Yi, L. "Cherimoya-like" polysilsequioxane microspheres with structure-enhanced spectral capability for passive daytime radiative cooling. *Mater. Today Commun.* **2022**, *32*, 104096.
(18) Hayase, G. Marshmallow-like Macroporous Silicone Monoliths as Reflective Standards and High Solar-Reflective Materials. *ACS Appl. Polym. Mater.* **2023**, *5* (7), 5280−5285.
(19) Hayase, G. Optical tactile sensor using scattering inside sol-gel-derived flexible macroporous monoliths. *Sens. Actuators A: Phys.* **2023**, *354*, 114253.
(20) Nagai, N.; Mizukami, F. Properties of boehmite and Al2O3 thin films prepared from boehmite nanofibres. *J. Mater. Chem.* **2011**, *21* (38), 14884−14889.
(21) Iijima, S.; Yumura, T.; Liu, Z. One-dimensional nanowires of pseudoboehmite (aluminum oxyhydroxide γ-AlOOH). *Proc. Natl. Acad. Sci. U. S. A.* **2016**, *113* (42), 11759−11764.
(22) Hayase, G.; Nonomura, K.; Kanamori, K.; Maeno, A.; Kaji, H.; Nakanishi, K. Boehmite Nanofiber−Polymethylsilsesquioxane Core−Shell Porous Monoliths for a Thermal Insulator under Low Vacuum Conditions. *Chem. Mater.* **2016**, *28* (10), 3237−3240.
(23) Hayase, G. Boehmite Nanofiber−Polymethylsilsesquioxane Composite Aerogels: Synthesis, Analysis, and Thermal Conductivity Control via Compression Processing. *Bull. Chem. Soc. Jpn.* **2021**, *94* (1), 70−75.
(24) Hayase, G.; Yoshino, D. CNC-Milled Superhydrophobic Macroporous Monoliths for 3D Cell Culture. *ACS Appl. Bio Mater.* **2020**, *3* (8), 4747−4750.
(25) Hotaling, N. A.; Bharti, K.; Kriel, H.; Simon, C. G., Jr. DiameterJ: A validated open source nanofiber diameter measurement tool. *Biomaterials* **2015**, *61*, 327−338.
(26) Schneider, C. A.; Rasband, W. S.; Eliceiri, K. W. NIH Image to ImageJ: 25 years of image analysis. *Nat. Methods.* **2012**, *9* (7), 671−675.
(27) van de Hulst, H. C. *Light Scattering by Small Particles*; Dover Publications: Mineola, NY, 1981, 63−171.
(28) Hayase, G.; Kugimiya, K.; Ogawa, M.; Kodera, Y.; Kanamori, K.; Nakanishi, K. The thermal conductivity of polymethylsilsesquioxane aerogels and xerogels with varied pore sizes for practical application as thermal superinsulators. *J. Mater. Chem. A* **2014**, *2* (18), 6525−6531.
(29) Kanamori, K.; Kodera, Y.; Hayase, G.; Nakanishi, K.; Hanada, T. Transition from transparent aerogels to hierarchically porous monoliths in polymethylsilsesquioxane sol-gel system. *J. Colloid Interface Sci.* **2011**, *357* (2), 336−344.
(30) Yu, H.; Zhou, C.; Wang, L.; Yang, C.; Li, S.; Wang, W. Enhancing optical performance of LED light diffusing plates through particle size and distribution control of organosilicone microspheres. *Opt. Mater.* **2024**, *151*, 115317.
(31) Oren, M.; Nayar, S. K. Generalization of Lambert's reflectance model. *Proceedings of the 21st annual conference on Computer graphics and interactive techniques*; Association for Computing Machinery: New York, 1994; pp 239−246. DOI: 10.1145/192161.192213.
(32) Trowbridge, T. S. Retroreflection from rough surfaces. *J. Opt Soc. Am* **1978**, *68* (9), 1225−1242.
(33) Trouvé, A.; Batonneau-Gener, I.; Valange, S.; Bonne, M.; Mignard, S. Tuning the hydrophobicity of mesoporous silica materials for the adsorption of organic pollutant in aqueous solution. *J. Hazard. Mater.* **2012**, *201*−*202*, 107−114.
(34) Catalanotti, S.; Cuomo, V.; Piro, G.; Ruggi, D.; Silvestrini, V.; Troise, G. The radiative cooling of selective surfaces. *Sol. Energy.* **1975**, *17* (2), 83−89.
(35) Bartoli, B.; Catalanotti, S.; Coluzzi, B.; Cuomo, V.; Silvestrini, V.; Troise, G. Nocturnal and diurnal performances of selective radiators. *Appl. Energy.* **1977**, *3* (4), 267−286.
(36) Raman, A. P.; Anoma, M. A.; Zhu, L.; Rephaeli, E.; Fan, S. Passive radiative cooling below ambient air temperature under direct sunlight. *Nature.* **2014**, *515* (7528), 540−544.
(37) Wang, K.; Luo, G.; Guo, X.; Li, S.; Liu, Z.; Yang, C. Radiative cooling of commercial silicon solar cells using a pyramid-textured PDMS film. *Sol. Energy.* **2021**, *225*, 245−251.
(38) Srinivasan, A.; Czapla, B.; Mayo, J.; Narayanaswamy, A. Infrared dielectric function of polydimethylsiloxane and selective emission behavior. *Appl. Phys. Lett.* **2016**, *109* (6), 061905.
(39) Zhou, L.; Song, H.; Liang, J.; et al. A polydimethylsiloxane-coated metal structure for all-day radiative cooling. *Nat. Sustain.* **2019**, *2* (8), 718−724.